Experimental Verification on Flexural Drift Capacity of Reinforced Concrete Wall with Limited Confinement

S. Takahashi, T. Ichinose and N. Izumi
Nagoya Institute of Technology, Japan

Y. Sanada
Osaka University, Japan

S. Matsubara
Toyohashi University of Technology, Japan

H. Fukuyama
Building Research Institute, Japan

H. Suwada
National Institute for Land and Infrastructure Management, Japan

SUMARRY
Many reinforced concrete (RC) structures were damaged in 2010 Chile Earthquake. Especially, damages of RC wall structures were reported. It was indicated that the low-confinement in the boundary element of these walls was a reason of their damages. Therefore, an experimental study was conducted to verify the flexural deformation capacity of RC wall with moderate confinement in boundary element. In this paper, ten specimens were tested. The test parameters were wall length, thickness, detailing and axial force. The detailing of ties did not satisfy the ACI requirements. Each specimen had a column at one end where an axial force was applied. All specimens failed in flexural compression after yielding of longitudinal bars. The observed flexural drift capacity was between 0.4 % and 1.2 %. A set of equations to predict the drift capacity is proposed, where hinge zone length is assumed 2.5 times of wall thickness.

Keywords: RC wall, Flexural drift capacity, Plastic hinge, Boundary element, Confinement

1. INTRODUCTION

In 2010 Chile Earthquake, many damages were observed in RC wall structures as shown in Fig. 1.1(National Earthquake Hazards Reduction Program 2010). These walls have low-confinement in boundary elements. This was indicated as one of the reasons of their damages. ACI 318 code (2008) admits two design approaches for evaluating detailing requirements at boundary element of RC wall resisting seismic force to prevent flexural compressive failure. One of the approaches is based on the displacement-based concept (Wallace et al 2002), where plastic hinge length is assumed as a half of wall length. If the compressive strain of concrete is expected to be larger than 0.003, the compressive zone is required to be reinforced according to the requirement of special boundary element with minimum volumetric ratio and spacing of confinement. This requirement is verified by Thomsen et al (2004), who tested walls with rectangular- and T-shaped cross section. Japanese code (2003) prescribes the ductility of RC wall based mainly on the ratio of the neutral axis depth to the wall thickness. This prescription is based on several experimental researches including those by Tabata et al (2003), who tested RC walls with rectangular cross section and large shear span length. This prescription can be approximated if we assume that the plastic hinge length is proportional to

(a) Damaged walls **(b) Boundary element**

Figure 1.1. Observed damages in Chile (National Earthquake Hazards Reduction Program 2010)

the wall thickness (Takahashi et al 2011).
The plastic hinge length is important for estimating deformation capacity, but there are various approaches to estimate it. Tabata et al evaluated deformation capacity of the wall supposing that the plastic hinge length was 0.3 times of wall length. On the other hand, Hiraishi (1984) used wall length as the plastic hinge length. Kabeyasawa et al (1983) idealized the wall of a story as three vertical elements with rigid beams at the top and bottom floor levels. In this model, the strain is assumed to be distributed uniformly within a story. Orakcal et al (2006) used the multiple-vertical-line-element (MVLEM) model and expressed a structural wall as a stuck of MVLEM elements. The strain distribution is also assumed to be uniform in each element. The height of the element is assumed 1/8 of story height in the first story.

The objective of this paper is to propose a way to estimate plastic hinge length and deformation capacity of RC walls. In this paper, 2.5 times of the wall thickness is proposed as the plastic hinge length. To verify this hypothesis, 10 specimens were tested. All of them don't satisfy ACI code but they are largely-advantageous in constructing. Test parameters were axial force, wall length, wall thickness, and with or without perpendicular wall.

2. EXPERIMENTAL PROGRAM

2.1 Specimens

Ten RC wall specimens with a boundary column on only one side were prepared in order to investigate the differences in deformation capacity. Fig. 2.1 shows the cross sections of the specimens used in this research. Each specimen is named as follows.

1. Perpendicular end wall: The first letter of specimen's name, P or N means with or without perpendicular wall, respectively. For example, PM5 in Fig. 2.1(g) has a perpendicular end wall 130 mm long and 60 mm thick. All the perpendicular end walls have single-layer reinforcement (D4@80, where D4 is a deformed bar with nominal diameter of 4 mm) and do not have confinement.
2. The ratio of wall panel length to wall thickness (l_{wp} /t): The second letter of specimen's name, S, M, and L expresses that l_{wp} /t ratio is 6, 12, and 18, respectively, where the wall panel length l_{wp} is defined excluding column. For example, the ratio of PM5 in Fig. 2.1(g) is 1200/100 = 12.
3. The ratio of neutral axis depth to wall thickness (c/t): The vertical arrows in Fig. 2.1 indicate the location of neutral axis, whose computation method will be shown later. The number of

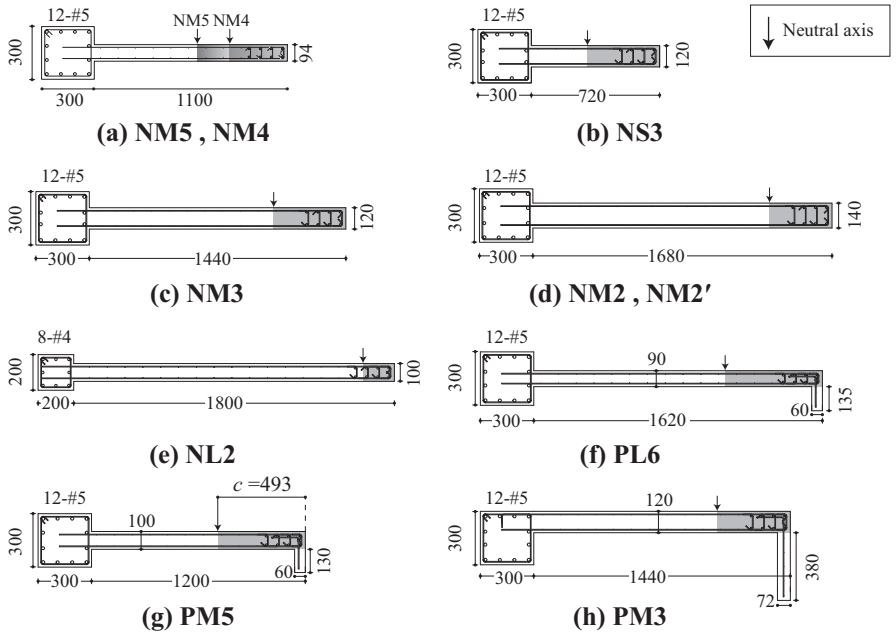

Figure 2.1. Specimens section [mm]

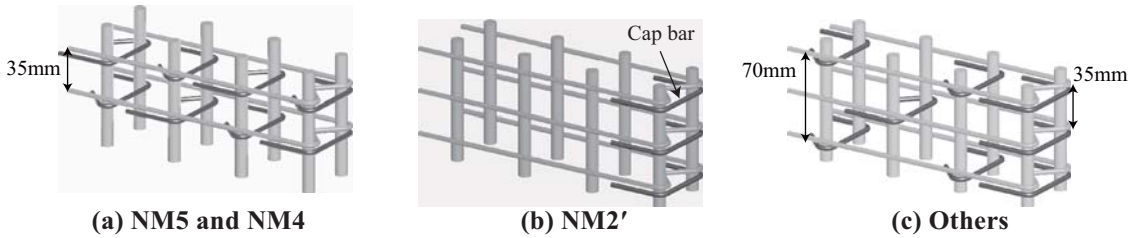

Figure 2.2. Isometric views of boundary elements

specimen's name expresses the approximate ratio of c/t. For example, the ratio of PM5 in Fig. 2.1(g) is 493/100 = 4.9. Although the section of NM5 and NM4 are identical as shown in Fig. 2.1(a), the locations of the neutral axis are different because of the difference of axial forces as shown later.

4. With or without cross-tie in boundary element: Fig. 2.2 shows the isometric views of the boundary elements. The horizontal bars have 135-degrees hook. The cap bars have 90-degrees hook at both ends as shown in Fig. 2.2(b), and its vertical spacing is 35 mm as shown in Fig. 2.2(c). The cross-ties have 90- and 135-degrees hooks as shown in Fig. 2.2(a), and are staggered with spacing of 70 mm as shown in Fig. 2.2(c) except for specimens NM5, NM4 and NM2′. Cross-ties in NM5 and NM4 are located at spacing of 35 mm as shown in Fig. 2.2(a). Specimen NM2′ does not have cross-ties as shown in Fig. 2.2(b).

The detailing of wall reinforcement for NM3 is shown in Fig. 2.3. The spacings of the horizontal and vertical bars are 35 mm and 100 mm, respectively. The reinforcement details of the wall panels of the other specimens are same as those in Fig. 2.3. Because the wall thickness of each specimen is different, the lateral and vertical wall reinforcement ratios vary from 0.54 to 0.84% and from 0.19 to 0.30%, respectively. The lengths of boundary elements are longer than a half of the length of neutral axis in most specimens as specified by the seismic requirements of the ACI 318[1]. In the vertical direction, cross-ties are provided from the bottom to1/3 of the clear height h as shown in Fig. 2.3. This value of $h/3$ is much shorter than the requirement of the ACI code. The spacing of cross-ties (70 mm in most specimens) does not satisfy the requirements of the ACI code, either. The cross sectional areas of cross-ties vary from 15% to 31% of the ACI code.

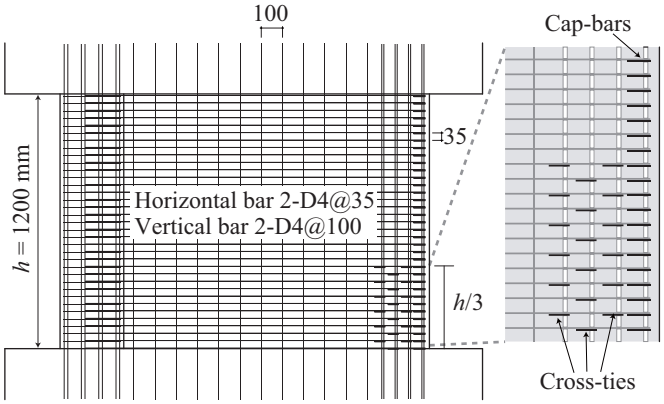

Figure 2.3. Elevation of specimen NM3

Table 2.1. Material properties

(a) Reinforcement

Bar	f_y (N/mm^2)	f_u (N/mm^2)	E_s (kN/mm^2)
D4	411(351)*	521(544)	173(192)
#3	391(376)	469(520)	199(188)
#4	367	503	183
#5	389(387)	559(563)	180(180)

*Numbers in parenthesis indicate the material properties for specimens NM4 and NM5

(b) Concrete

Specimen	f_c' (N/mm^2)	E_c (kN/mm^2)	f_r (N/mm^2)
NS3, NM3	38.3	28.4	2.65
NM2, NM2′	37.8	27.8	2.45
NL2, PL6 PM5, PM3	37.6	28.6	3.07
NM5, NM4	33.4	23.9	2.55

The clear heights of specimens NM4 and NM5 are 1000 mm, while those of the other specimens are 1200mm as shown in Fig. 2.3. Eight #3 longitudinal bars are provided in the boundary element of all specimens (Fig. 2.2). Twelve #5 longitudinal bars are provided in the boundary column except that of specimen NL2, where eight #4 bars are provided (Fig. 2.1e) so that the longitudinal reinforcement ratio (2.5%) is similar to that of the other specimens.

All specimens are designed to fail in flexure; the shear to flexural capacity ratios vary from 1.2 to 2.3, where the flexural and shear capacities are calculated based on the AIJ Standards (2010) and ACI code (2008), respectively. Material properties of steel bars are indicated in Table 2.1(a), where f_y is the yield strength, f_u is the tensile strength, and E_s is the elastic modulus. Material properties of concrete are indicated in Table 2.1(b), where f_c' is the compressive strength, E_c is the elastic modulus, and f_r is the modulus of rupture.

2.2 Test setup

Figure 2.4 shows the test setup. Lateral force was applied by hydraulic jack to a stiff loading steel beam fastened to specimen. All specimens had stiff RC stubs at both top and bottom for fixing with loading frame. No axial force was applied for NM4. For the other specimens, two vertical hydraulic jacks were force-controlled so that the moment around at the center of the boundary column is zero as shown in Fig. 2.4. The amount of the axial force was approximately 20% of the axial capacity of boundary column ($f_c' \cdot A_g$), where A_g is gross cross sectional area of column. The applied axial load was approximately 240 kN for NL2, 400 kN for NM5 and 540 kN for the other specimens. Horizontal load was applied 2425 mm above the bottom of the wall panel for NM5 and NM4 (Fig. 2.4). Height of horizontal load was 2525 mm for the other specimens. The shear span ratio of NL2 is 2525/2000 = 1.26, which is the smallest. The shear span ratio of NS3 is 2525/1020 = 2.48, which is the largest.

3. OBSERVED DAMAGE AND DEFLECTION COMPONENT

Figure 3.1(a) shows the lateral load-drift relationship of NL2. Lateral drift, R, is defined as the ratio of measured lateral displacement, to specimen height, h. The displacement was measured at the top of the clear height in all specimens. During the positive loading (column in tension), the maximum strength (530 kN) was observed at +1.2% drift level. The strength was 1.1 times the analytical flexural strength. Between the drift levels of +2% and +3%, strength decreased rapidly. During the negative loading direction (column in compression), the maximum strength (280 kN) was observed

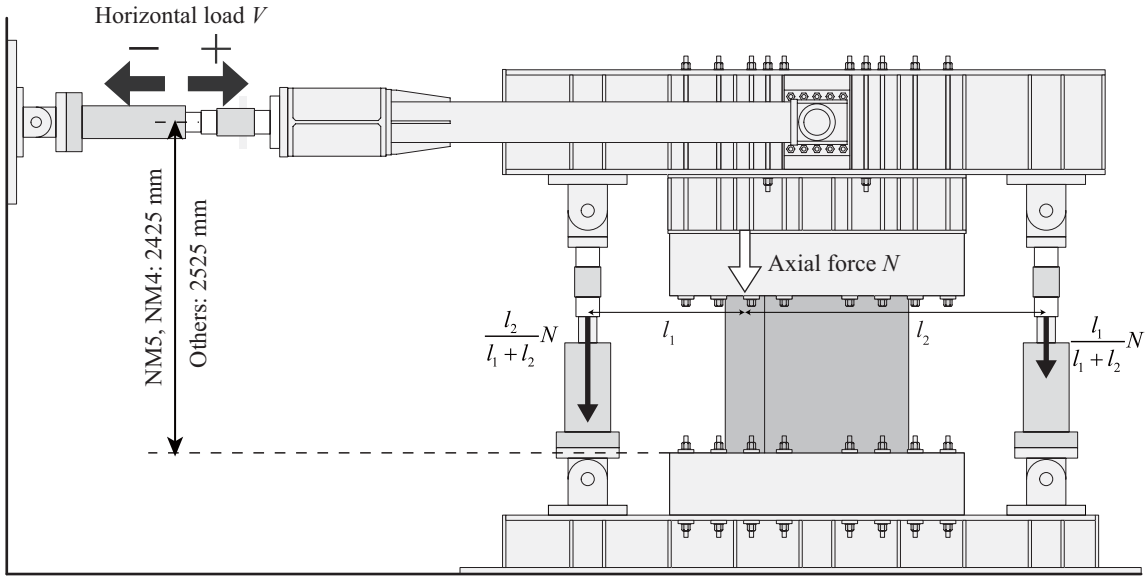

Figure 2.4. Loading setup

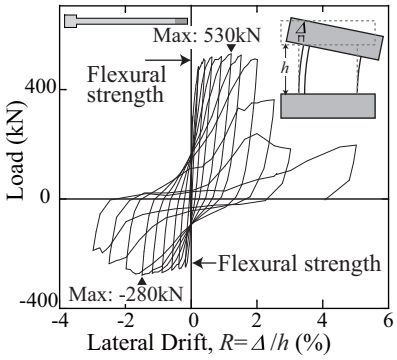

(a) Load versus lateral drift

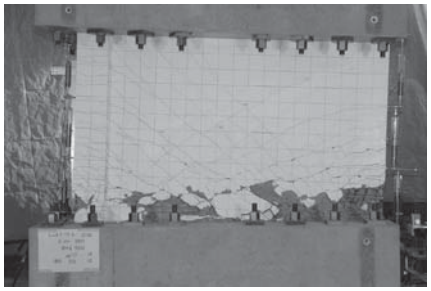

(b) Failure at maximum drift

(c) Buckling of reinforcement

Figure 3.1. Test result of specimen NL2

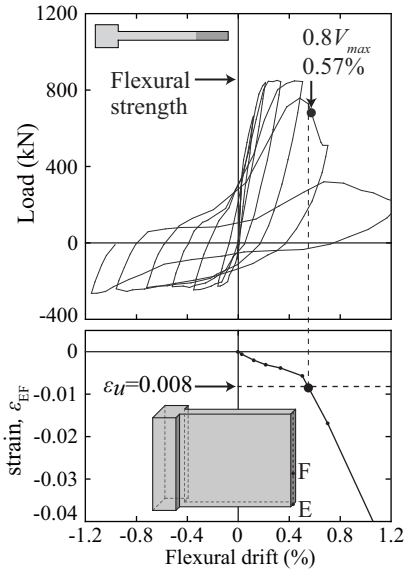

(a) Specimen NM3

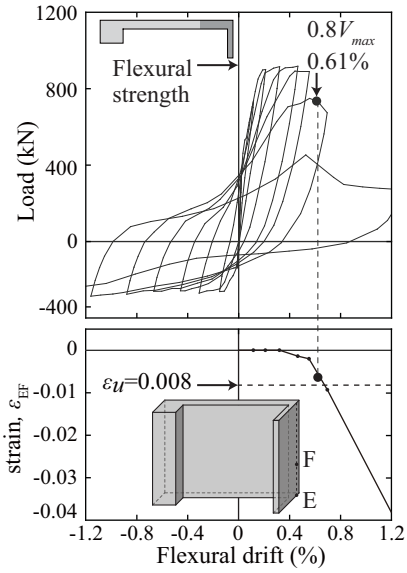

(b) Specimen PM3

Figure 3.2. Load and strain versus flexural drift

at -1.5% drift level. The strength was 1.2 times the analytical flexural strength.
Figure 3.1(b) shows specimen NL2 at the end of experiment, at 5% drift level. The spalling of concrete started at the bottom right corner of the wall panel at +2% drift level. The spalled zone extended toward the column till +3% drift level. On the other hand, the concrete of the boundary column slightly spalled during the negative loading, but not during the positive loading even at +5% drift level. Fig. 3.1(c) shows the buckling of the longitudinal bars (8-#3) in the boundary element at 3% drift level. The buckled bars fractured in tension between the drift levels of -2% and -3%.

Load and strain versus flexural drift of NM3 and PM3 are shown in Fig. 3.2 to investigate the effect of perpendicular wall on flexural drift capacity. Flexural drift is calculated according to Orakcal et al (2006). Flexural drift at 80% of maximum strength V_{max} (the black circle in Fig. 3.2) is defined as flexural drift capacity in this paper. Difference between these two specimens is the existence of perpendicular wall. The drift capacities of NM3 (0.57%) and PM3 (0.61%) were similar. The compressive failure of the perpendicular wall of PM3 occurred before the lateral strength degradation started. Because the perpendicular wall is provided with no confinement (Fig. 2.1), the compressive ductility of this wall was very limited at the ultimate drift. Therefore, the contribution of perpendicular wall should be ignored in evaluating the drift capacity. The vertical axes of lower part of Fig. 3.2 show the average strain at the compression edge (strain between E and F). The plastic hinge lengths of these two specimens, which will be evaluated later as 2.5 times wall thickness (300 mm), are similar to the length between E and F (400 mm). The strains at the ultimate drifts (the black circles in the figures) were approximately 0.008, which agrees with the ultimate

strain of concrete, ε_u, computed later considering the confinement effect.

4. FLEXURAL DRIFT CAPACITY

4.1 Simplification of plastic deformation

In this paper, flexural drift capacity is decomposed into elastic and plastic components ($R_u = R_y + R_p$) as shown in Fig. 4.1(a). The curvature at yielding ϕ_y is computed based on the yield strain of longitudinal reinforcement.

$$\phi_y = \frac{\varepsilon_y}{d - c} \tag{4.1}$$

where ε_y: yield strain of reinforcement;
d: effective depth defined as the distance between compression edge and center of column; and
c: neutral axis depth computed from Eqn. 4.2.

$$c = \frac{C}{0.85\beta_1 f_c' t} \tag{4.2}$$

where C = compressive force of concrete computed from Eqn. 4.3;
β_1= reduction factor to determine neutral axis;
f_c' = compressive strength of concrete; and
t = wall thickness.

$$C = N + \sum A_{st} f_y - \sum A_{sc} f_y \tag{4.3}$$

where N = applied axial load;
A_{st} = gross sectional area of longitudinal bars in tension;
A_{sc} = gross sectional area of longitudinal bars in compression; and
f_y = yield strength of longitudinal bar.

Theoretically, Eqn. 4.2 is effective at ultimate state and ineffective at yielding. However, this difference may be negligible because the amount of the wall reinforcements is much smaller than that in the boundary column.

In this research, linear distribution was used for elastic curvature (Fig. 4.1a). Therefore, the elastic drift R_y is computed from Eqn. 4.4.

$$R_y = \frac{\Delta_{fy}}{h} = \left(\frac{h}{2} - \frac{h^2}{6a}\right) \cdot \phi_y \tag{4.4}$$

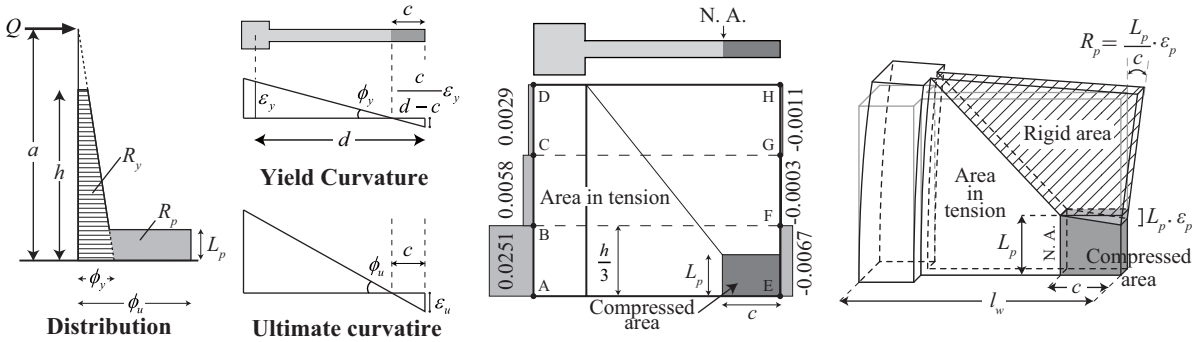

(a) Assumed distribution of curvature **(b) Measured strain of NM4** **(c) Plastic deformation**

Figure 4.1. Elastic and plastic deformations

where δ_{fy} = flexural displacement at yielding;
a = shear span length; and
h = specimen's clear height.
The ultimate curvature ϕ_u is computed based on the ultimate strain of concrete (Fig. 4.1a), where ε_u is ultimate compressive strain of concrete defined later:

$$\phi_u = \frac{\varepsilon_u}{c} \tag{4.5}$$

The plastic drift is computed using plastic hinge length L_p.

$$R_p = L_p \cdot \left(\phi_u - \phi_y\right) \tag{4.6}$$

Substituting Eqns. 4.1 and 4.5 into Eqn. 4.6 leads to the equation to compute the plastic drift.

$$R_p = \frac{L_p}{c} \cdot \left(\varepsilon_u - \frac{c}{d-c}\varepsilon_y\right) \tag{4.7}$$

Figure 4.1(b) shows the strain distribution measured using LVDTs along the clear height of specimen NM4 when the lateral force decreased to 80% of the maximum strength. On the compressive side (the right edge), the strain localized between points E and F, whereas the strain between F and G or G and H was quite small. On the tensile side (the left edge), even the strain between C and D exceeded the yield strain ($0.0029 > \varepsilon_y = 0.002$). It is concluded that, for plastic deformation, the compressed area is limited near the bottom of the wall as indicated by the shaded rectangle in Figs. 4.1(b) and (c) whereas the area in tension is trapezoidal. The hatched area in Fig. 4.1(c) is assumed as rigid. The strain at the compressed edge in Fig. 4.1(c) is assumed to be uniformly ε_p that equals the term inside the parenthesis of Eqn. 4.7:

$$\varepsilon_p = \varepsilon_u - \frac{c}{d-c}\varepsilon_y \tag{4.8}$$

where the second term is the strain caused by the elastic deformation. In this paper, ε_p is called plastic component of ultimate strain. Note that the rigid area in Fig. 4.1(c) rotates

$$R_p = \frac{L_p}{c}\varepsilon_p \tag{4.9}$$

around the neutral axis. Therefore, the height of the compressed area in Fig. 4.1(c) can be regarded as the plastic hinge length L_p. The deformation shown in Fig. 4.1(c) agrees with the observed crack patterns and is similar to that proposed by Hiraishi (1984).

There are two unknown parameters, L_p and ε_p, in Eqn. 4.9. In the following sections, these parameters are examined using the tested specimens. Specimens tested by Wallace et al. (2002) and Tabata et al. (2003) are used because flexural deformations of specimens are reported.

4.2 Plastic component of ultimate strain

The broken lines in Fig. 4.2(a) show the stress-strain relationships of confined and unconfined concrete in NS3 evaluated by Saatcioglu and Razvi model (1992), which is applicable to rectangular sections. Figure 4.2(b) shows the boundary element of Specimens including No. 2 and 3 of Tabata et al. (2003) where the shaded zone is assumed to be confined. Regarding specimen NM3, The confining pressure on the shaded zone in x-direction is computed assuming that the horizontal bars are 100% effective. The confining pressure in y-direction is computed assuming that the cross-ties are 100% effective while the cap bars at the wall end with 90-degree hooks are 50% effective because the observed strain of the cap bars were approximately one half of yield strain. Although only cap bars are provided to NM2′, the shaded area is again assumed to be confined. The confining

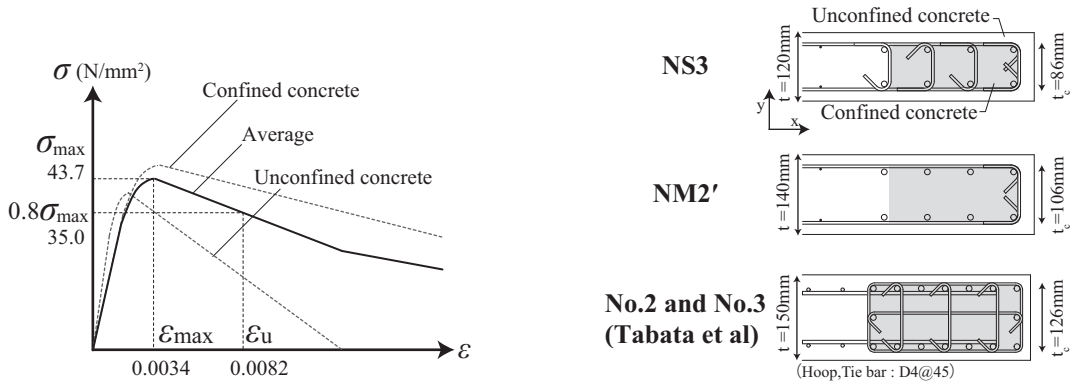

(a) Stress-strain model for NS3 **(b) Assumed confined regions**

Figure 4.2. Ultimate compressive strain

pressure in y-direction is computed assuming that the cap bars are 50% effective.
The solid line in Fig. 4.2(a) shows the average stress-strain relationship of the boundary element calculated as the weighted average of confined and unconfined concrete.

$$\sigma = \sigma_c \cdot \frac{t_c}{t} + \sigma_u \cdot \frac{t - t_c}{t} \tag{4.10}$$

where σ_c: stress of confined concrete;
t_c: the center-to-center distance between the horizontal wall bars (Fig. 4.5a); and
σ_u: stress of unconfined concrete.

The ultimate concrete strain ε_u is defined as the strain when the average stress of concrete decrease to 80% of the maximum strength. The ultimate strain of Specimen NM2′ without cross-tie is 0.0066 while those of the other specimens are between 0.0078 and 0.0084. The ultimate strains of the specimens of Wallace et al. (2002) are around 0.008 except that the strain of TW2 is 0.0112. Although the confinement ratio of No. 2 and No. 3 is higher than those of others, its ultimate strain is 0.008 because its concrete strength was high (70 MPa). The strain at compressive edge when tensile reinforcement bars yield shown in Fig. 4.1(a) (the second term in Eqn. 4.8) is approximately 0.001 in most specimens. Therefore, ε_p in Eqn. 4.9 is approximately 0.008–0.001=0.007 for all specimens except NM2′ and TW2.

4.3. Plastic hinge length

As discussed in Introduction, Wallace et al. (2002) and Tabata et al. (2003) assumed that L_p is equal to $0.5l_w$ and $0.3l_w$, respectively, where l_w is wall length. From Fig. 4.3, the plastic hinge length of NL2 is much smaller than $0.3l_w$. ACI 318 requires that the special boundary region shall be longer than $a/4$ where a is shear span length. This requirement implies that L_p in Fig. 4.3 equals $a/4$. The plastic hinge length is also smaller than $a/4$ in Fig. 4.3.

Markeset et al. (1995) conducted uniaxial compression tests of plain concrete prisms with various lengths and sectional dimensions. They observed that compressive failure is quite limited within

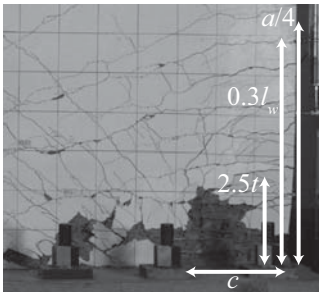

Figure 4.3. Failure of NL2 at 2.5% drift

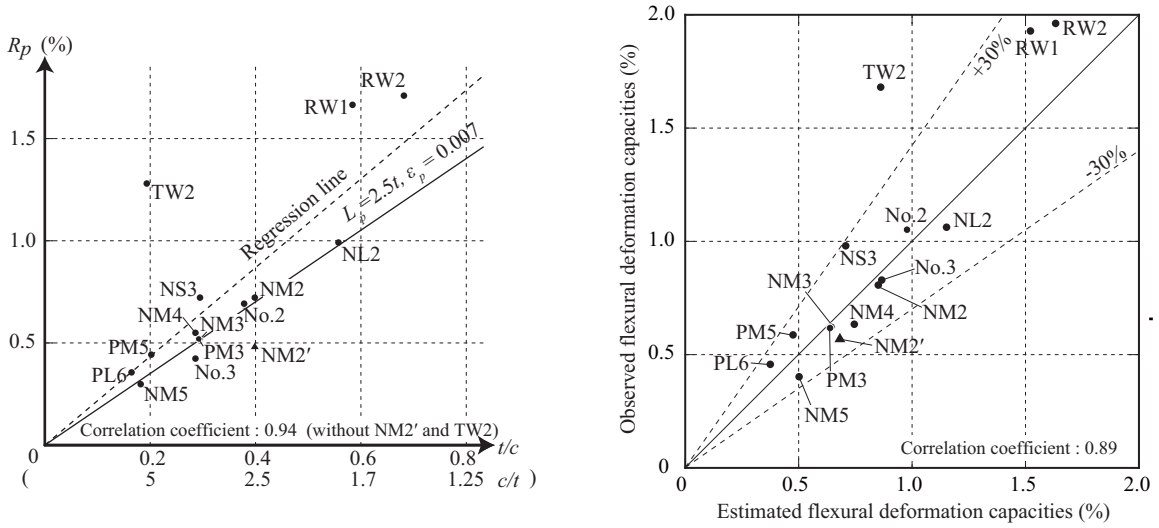

(a) Relationship between R_p and t/c **(b) Estimated and observed flexural drift capacities**

Figure 4.4. Comparison between the estimated and observed drift

certain length. They concluded that the failure length was 2.5 times of the shorter side length of the compressed section. In this research, wall thickness t is shorter than neutral axis depth c in all specimens. In Fig. 4.3, the damage length seems almost 2.5 times of wall thickness. Therefore, 2.5t is used for plastic hinge length L_p in this research. It should be also noted that even in specimen NM2 with largest thickness (t = 140 mm), the damage of concrete was limited within the height of confinement (400 mm). It is therefore concluded that the height of confinement may be limited to 3t, if the expected compressive strain is not larger than 0.008.

Figure 4.4(a) shows the relation between R_p and t/c. The correlation coefficient is 0.94. The broken line in Fig. 4.4(a) shows the regression line. The solid line shows R_p estimated from L_p = 2.5t and ε_p = 0.007. The solid line reasonably agrees with the regression line, which implies that the assumption of L_p = 2.5 t is appropriate.
Figure 4.4(b) compares the observed and estimated flexural drift capacities ($R_u = R_y + R_p$). All test data except TW2 are within 30% from the estimated drift capacities. The observed drift of TW2 is much larger than the estimated value. The observed compressive failure zone of TW2 was also much wider than L_p = 2.5t. Similar tendencies are observed for the test results of Paulay et al. (1993), which are not plotted in Fig. 4.4(b) because their flexural drift capacities are not reported. These discrepancies may be attributable to the difference of confinement because specimen TW2 and the specimens tested by Paulay et al. (1993) almost satisfied the requirements of ACI 318. On the other hand, the cross-sectional areas of the confining bars provided to the other specimens in Fig. 4.4(b) were less than half of the requirement. It is concluded that L_p = 2.5t is valid if the confinement of boundary element is less than a half of that required by the seismic provisions of ACI 318. Otherwise, the equation tends to underestimate the capacity.

5. CONCLUSIONS

Test results of ten RC walls were described. Based on the experimental results and analytical work presented in this paper, the following conclusions are obtained.

1. All of tested RC walls with limited confinement in boundary element failed in compression after flexural yielding. The observed flexural drift capacity was between 0.4 % and 1.2 %.

2. Plastic components of flexural drift can be modeled as shown in Fig. 4.1(c), where the length of compression zone L_p is 2.5 times of the wall thickness (L_p = 2.5t), if the depth of neutral axis is longer than the wall thickness and the confinement of the boundary element is less than a half of that required by the seismic provisions of ACI-318 code.

3. Ultimate flexural drift is defined as the drift when the lateral force decreased to 80% of maximum lateral strength. Ultimate flexural drift can be computed as the sum of Eqns. 4.4 and 4.7, where ε_u shall be determined as shown in Fig. 4.2(a) considering the confinement effect.

4. The detailing of the boundary element shown in Fig. 2.2(c) with the height of confined area 3*t* is sufficient to obtain ultimate strain of ε_u =0.008.

5. The effect of perpendicular wall on ultimate drift is negligible if the wall is not confined.

ACKNOWLEDGEMENT

This work was financially supported by MLIT (Ministry of Land, Infrastructure, Transport and Tourism) Japan. Data provided by Drs. Tabata, Nishihara and Suzuki of Ando Corporation are greatly appreciated.

REFERENCES

American Concrete Institute (2008), ‘‘Building code requirements for structural concrete.’’ *ACI 318-08*, Farmington Hills, Michigan.

Architectural Institute of Japan (2010), “AIJ Standard for Structural Calculation of Reinforced Concrete Structures.” Maruzen, Tokyo.

Hiraishi H. (1984), “Evaluation of Shear and Flexural Deformations of Flexural Type Shear Walls,” *Bulletin of the New Zealand National Society for Earthquake Engineering*, Vol. 17, No. 2, pp. 135-144.

Kabeyasawa T., Shiohara H., Otani S., and Aoyama H. (1983), “Analysis of the Full-Scale Seven-Story Reinforced Concrete Test Structure,” *Journal of the Faculty of Engineering*, University of Tokyo (B), Vol. 37, No. 2, pp. 431-478.

Markeset, G. and Hillerborg, A. (1995), “Softening of concrete in compression localization and size effects,” *Cement and Concrete Research*, Vol. 25, No.4, pp. 702-708.

National Earthquake Hazards Reduction Program (2010), Executive Summary on Chile Earthquake Reconnaissance Meeting, NEHARP Library, http://www.nehrp.gov/library/ChileMeeting.htm

National Institute for Land and Infrastructure Management (2003), “Design Guidelines for High-raise RC Frame-wall Structures.” Kaibundo, Tokyo.

Orakcal, K., and Wallace, J. W. (2006), “Flexural Modeling of Reinforced Concrete Walls-Experimental Verification,” *ACI Structural Journal*, Vol. 103, No. 2, pp. 196-206.

Paulay, T., and Priestley, M. J. N. (1993), “Stability of Ductile Structural Walls,” *ACI Structural Journal*, Vol. 90, No. 4, pp. 385-392.

Saatcioglu, M., and Razvi, S. R. (1992), “Strength and Ductility of Confined Concrete,” *J. Struct. Eng*., ASCE, Vol. 118, No. 6, pp. 1590-1607.

Tabata T, Nishihara H, and Suzuki H (2003), “Ductility of Reinforced Concrete Shear Walls without Column Shape,” *Proceedings of the Japan Concrete Institute*, Vol. 25, No. 2, pp.625-630. (In Japanese)

Takahashi S., Yoshida K., Ichinose T., Sanada Y., Matsumoto K., Fukuyama H., and Suwada H. (2011), “Flexural Deformation Capacity of RC Shear Walls without Column on Compressive Side,” *J. Struct. Constr. Eng*., AIJ, Vol. 76, No. 660, pp.371-377. (In Japanese)

Thomsen, J. H., and Wallace, J. W. (2004), “Displacement-Based Design of Slender Reinforced Concrete Structural Walls-Experimental Verification,” *J. Struct. Eng*., ASCE, Vol. 130, No. 4, pp. 618-630.

Wallace, J. W., and Orakcal, K. (2002), “ACI 318-99 Provisions for Seismic Design of Structural Walls,” *ACI Structural Journal*, Vol. 99, No. 4, pp. 499-508.